ISPRS Journal of Photogrammetry and Remote Sensing 91 (2014) 17–28

Contents lists available at ScienceDirect

ISPRS Journal of Photogrammetry and Remote Sensing

journal homepage: www.elsevier.com/locate/isprsjprs

Empirical comparison of noise reduction techniques for NDVI time-series based on a new measure

Ryo Michishita [a], Zhenyu Jin [a], Jin Chen [a], Bing Xu [a,b,c,*]

[a] State Key Laboratory of Remote Sensing Science, College of Global Change and Earth System Science, Beijing Normal University, Beijing 100875, PR China
[b] School of Environment, Tsinghua University, Beijing 100084, PR China
[c] Department of Geography, University of Utah, Salt Lake City, UT 84112, USA

ARTICLE INFO

Article history:
Received 19 August 2013
Received in revised form 11 January 2014
Accepted 14 January 2014
Available online 4 March 2014

Keywords:
Vegetation index
Multitemporal
MODIS
Land cover
Monitoring

ABSTRACT

This study empirically compared noise reduction techniques for the normalized difference vegetation index (NDVI) time-series based on a new absolute measure using a time-series of 16-day composite NDVI images extracted from the Terra Moderate Resolution Imaging Spectroradiometer (MODIS) products covering the Poyang Lake area in China. We proposed an approach to accurately extract representative NDVI temporal profiles for the 12 land cover cluster types by clustering profiles, selecting optimal number of clusters, merging and labeling clusters, and selecting the representative NDVI profiles. The geometric average of the mean average distance between the reconstructed profile and the raw profiles, and the mean average distance between the reconstructed profile and the upper envelope ($D_g(nr,c)$) was selected as the most appropriate measure substitutive to RMSE for the evaluation of the noise reduction effects, when the 'true' profiles were not available. The running median, mean value, maximum operation, end point processing, and Hanning smoothing (RMMEH) filter and iterative Savitzky–Golay filter were the two most appropriate noise reduction techniques for the NDVI temporal profiles of the study area in the evaluation of noise reduction effects by the seven techniques. The robust framework using the proposed approach for the accurate extraction of representative NDVI temporal profiles and ($D_g(nr,c)$) in this study, is applicable in the evaluation of noise reduction effects using different techniques and in other study areas.

1. Introduction

The time-series normalized difference vegetation index (NDVI) images derived from multi-temporal coarse remotely sensed data with coarse spatial resolution have been used for characterizing vegetation phenology and land cover changes (Moody and Johnson, 2001). NDVI has been most widely used to link to the structural properties and photosynthetic activity of vegetation (Roderick et al., 1999; Lu et al., 2001; Beck et al., 2006). Due to the response of phenological dynamics in terrestrial ecosystems to climatic and hydrologic dynamics, NDVI time-series have been utilized to reveal global carbon, nitrogen, and water cycles, spatial shift of bio-climatic zones, and phenological changes in response to climate fluctuations and human activities (Myneni et al., 1997; Jönsson and Eklundh, 2002; Bradley et al., 2007). The derivation of phenological metrics, decomposition of temporal NDVI profiles into inter-annual, seasonal, and abrupt trends, and multi-temporal classification are three major analytical approaches using the NDVI time-series (Cleveland et al., 1990; Knight et al., 2006; Verbesselt et al., 2010; Zhang et al., 2012). Recently, the number of studies using the NDVI time-series in wetland ecosystems has increased aiming at understanding the detailed temporal dynamics in wetland cover changes such as inundation and phenology of wetland vegetation (Rodgers et al., 2009).

It is well known that the effect of cloud contamination, atmospheric variability of dust, ozone, or aerosols, bidirectional effects, sensor viewing angles, solar angles, snow cover, and problems with instruments often degrade the NDVI time-series (Atkinson et al., 2012). Sudden drops, with abnormally low NDVI values in the NDVI time-series generated by these effects, have often prevented accurate analysis of the dynamics in land and water cover changes. Although the time-series NDVI images are often composites for a period of certain days to reduce these effects, significant residual

* Corresponding author. Present address: College of Global Change and Earth System Science, Beijing Normal University, Beijing 100875, PR China. Tel.: +86 10 6279 3906; fax: +86 10 6278 5687.
E-mail address: bingxu@tsinghua.edu.cn (B. Xu).

http://dx.doi.org/10.1016/j.isprsjprs.2014.01.003
0924-2716/

effects remain in them (Ma and Veroustraete, 2006). Since the accuracy of the time-series analysis of NDVI images depends on the quality of the input data, reduction of these effects from the NDVI time-series is critically important.

To reconstruct high quality NDVI time-series, a number of techniques have been developed and applied over the last 25 years. These techniques can generally be categorized into four broad groups: (1) threshold-based techniques, such as the best index slope extraction (BISE) filter (Viovy et al., 1992); (2) Fourier-based fitting techniques, such as fast Fourier transformation (Sellers et al., 1994); (3) asymmetric function fitting techniques, such as the asymmetric Gaussian function (AG) fitting (Jönsson and Eklundh, 2002), the weighted least squares linear regression (Swets et al., 1999), double logistic function (DL) fitting (Beck et al., 2006), ARMD3-ARMA5 (ARM3-5) filter (Filipova-Racheva and Hall-Beyer, 2000), and iterative Savitzky-Golay (GL) filter (Chen et al., 2004); and (4) iterative simple mathematical operation techniques such as the 4253H Twice (4253HT) filter (Velleman, 1980), maximum-value iteration (MVI) filter (Ma and Veroustraete, 2006), and RMMEH filter (Jin and Xu, 2013). Several studies have provided useful information in choosing appropriate noise reduction techniques for the NDVI time-series by comparing the performance of multiple noise reduction techniques (Dijk et al., 1987; Jönsson and Eklundh, 2004; Hird and McDermid, 2009). Their inconsistent results have suggested that effects of noise reduction varied in different land cover types and study areas, therefore evaluation of noise reduction effects might be necessary before conducting each application.

The effects of noise reduction have been evaluated through the analysis of NDVI temporal profiles. A number of studies have manually selected certain number of sample profiles for each land cover class (Bradley et al., 2007), or randomly extracted large number of pixels then manually classified them into land cover classes (Chen et al., 2004). However there have been a few studies on time-efficient approaches for the extraction of representative temporal profiles that are comprehensive in the entire study area, even though the extraction is an essential step for accurate evaluation of noise reduction effects.

Most of the studies evaluating the performance of these noise reduction techniques have depended on visual interpretation of NDVI profiles. A few studies have quantitatively evaluated the noise reduction performance based on different criteria, such as the root mean square error (RMSE) between modeled and noise-added profiles, and the difference of phenological metrics derived from modeled and noise-added profiles (Hird and McDermid, 2009), by regarding the modeled profiles as 'true' profiles. However, realistic noise-added profiles are extremely difficult to generate, because of the influence of the actual noise by a number of factors described above. In actual NDVI temporal profiles, the amplitude and frequency of positive and negative noise are different, and in general noise are biased negatively (Ma and Veroustraete, 2006; Julien and Sobrino, 2010).

Instead of using noise-added profiles, Beck et al. (2006) evaluated the effects of noise reduction using observed and reconstructed profiles. Although it was based on the RMSE between the observed and reconstructed profiles, the evaluation was rather subjective because there were no "true" noise-free profiles that could be derived from the observed profiles (Julien and Sobrino, 2010). In such situation, the RMSE was not an appropriate measure for comparing the observed and reconstructed profiles, although the RMSE is an absolute measure when the modeled profiles were compared with the reconstructed profiles derived from synthesizing noise-added profiles. Instead of the RMSE, two noise reduction measures calculated from the observed and reconstructed NDVI profiles were proposed in Julien and Sobrino (2010). However, the appropriateness of these measures for the evaluation of noise reduction effects was not examined. Thus, there is a significant need for the development of an absolute measure for the evaluation of noise reduction effects using observed and reconstructed NDVI time-series.

This study aims to empirically compare noise reduction techniques for NDVI time-series based on a new absolute measure using a time-series of 16-day composite NDVI images extracted from the Terra Moderate Resolution Imaging Spectroradiometer (MODIS) products covering the Poyang Lake area in China. First, an approach to the extraction of representative NDVI temporal profiles is explored. Using the modeled profiles generated from the extracted profiles, we develop a robust measure for the absolute evaluation of noise reduction effects when 'true' profiles are unavailable. Finally, the seven noise reduction techniques, including those applied in Hird and McDermid (2009) and the running median, mean value, maximum operation, end point processing, and Hanning smoothing (RMMEH) filter (Jin and Xu, 2013), a simple automated compound filter that does not require ancillary data, are compared in the evaluation of noise reduction effects.

2. Study area and datasets

2.1. Study area

The study area is located in the Poyang Lake area in China, covering approximately 16,900 km^2 (Fig. 1). We conducted a number of remote sensing studies to monitor environmental changes in this area, such as urbanization, inter-annual changes in lake inundation, and seasonal changes in wetland vegetation cover (Hui et al., 2008; Michishita et al., 2012a; Michishita et al., 2012b; Michishita et al., 2012c; Wang et al., 2013; Chan and Xu, 2013). Poyang Lake (116°13′E, 29°9′N), the largest freshwater lake in China located in the northern part of Jiangxi Province, shows a unique hydrological pattern throughout the year. The water from five major rivers fills the lake and inundates all the lowland marshlands between April and June. The flood backflows from the Yangtze River increase the water levels in the lake enough to reach their peaks between July and September. Vast areas with wetland vegetation emerge after the lake water subsides in October and November. Disconnected small lakes maintain different water levels between December and February (Guo et al., 2005).

This study area is suitable for the analysis because of its richness in the variety of land use and land cover types. Vegetated wetlands are dominated by the *Carex*, *Miscanthus*, and *Phragmites* species. Other wetland components include mud, sands, and dead algae. Flatlands between the lake and needle leaf forests are used for rice paddies in the central and southern part of the lake, and for cotton fields in the northern part. Oil seed rapes are planted in the western and northwestern parts of the lake. Two large cities with populations of about five million, Nanchang and Jiujiang, are located in the northwestern and southwestern parts of the lake, respectively (Fang et al., 2006).

2.2. Datasets

We used 263 NDVI time-series images extracted from the Terra MODIS Vegetation Indices 16-Day L3 Global 250 m (MOD13Q1) products (version 005) covering the study area over a period of 11 years from October 15, 2000 to March 5, 2012. These products were acquired from the Reverb | ECHO operated by NASA (<http://reverb.echo.nasa.gov/reverb/>). The NDVI images in the products were derived from the surface reflectance data that were atmospherically corrected taking into account the effects of molecule scattering, ozone absorption, and aerosols (Huete et al., 2002). Quality assurance images were also extracted for the performance

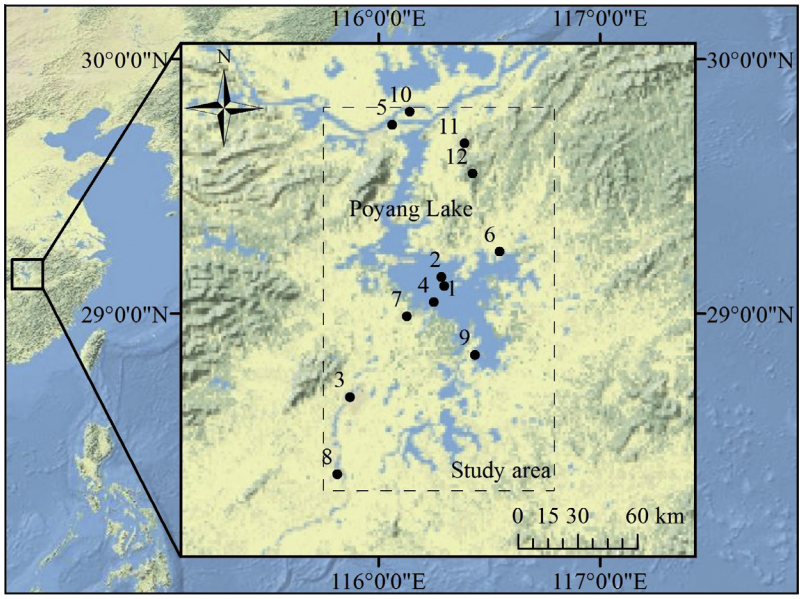

Fig. 1. Study area: Poyang Lake area, China. Points 1–12 are the sample locations for the comparisons chosen through the cluster detection, labeling of the clusters, and calculation of a representativeness index from the NDVI time-series.

of the SG filter. All data used in this study were reprojected to Universal Transverse Mercator (Zone 50 N, WGS-84) and stacked into single layered image.

This study used supplemental materials to define cluster labels, merge and label clusters, and assess labeling accuracy in the selection of representative NDVI profiles, and to select the pixel locations of inter-annual and seasonal land cover change events. They included: (1) field records of the representative land cover types and their changes around the Poyang Lake in December, 2007 and April and May, 2008 (Michishita et al., 2012a,b,c); (2) 30 time-series Landsat-5 Thematic Mapper (TM) and Landsat-7 Enhanced Thematic Mapper Plus (ETM+) images observed between 1987 and 2011 (Appendix 1); (3) two high accuracy land cover classification maps derived from the ETM+ image acquired on August 22, 2000 (Niu et al., 2009; provided by the Institute of Remote Sensing Applications, Chinese Academy of Sciences; Appendix 2 (a)) and the TM image derived from the TM image acquired on October 26, 2009 (Gong et al., 2013; downloaded from the Finer Resolution Observation and Monitoring – Global Land Cover website, URL: http://data.ess.tsinghua.edu.cn/index.html; Appendix 2 (b)); (4) multi-temporal high spatial resolution images from Google Earth and Microsoft Bing Maps acquired in 2002, 2003, and 2005–2011 (Appendix 3); (5) land use map in the Jiangxi Map Collection (Editing Committee of Jiangxi Map Collection, 2008); and (6) results of interviews with the local residents and researchers on agriculture and wetlands (Appendix 4 for the interview form).

3. Method

Fig. 2 summarizes the overall procedure we followed in this study. The process started with the exploration of an approach for extracting representative NDVI temporal profiles (Step 1 in Fig. 2). In the second step (Step 2 in Fig. 2), we developed a measure of noise reduction effects when the 'true' profiles were not available. Finally, the effects of noise reduction by seven techniques were evaluated and compared both visually and quantitatively in the third step (Step 3 in Fig. 2). Every step in Fig. 2 is described in details below.

3.1. Exploration of an approach to extracting representative NDVI temporal profiles

Extraction of a set of NDVI temporal profiles that are representative and comprehensive in the study area from the original time-series NDVI images is an important step in the evaluation of noise reduction effects. This study explored an approach to extracting representative NDVI temporal profiles, consisting of NDVI profile clustering, selection of optimal number of clusters, cluster merging, labeling accuracy assessment, and selection of representative NDVI profiles. Details for each step are described below.

The iterative self-organizing data analysis (ISODATA) algorithm, an unsupervised clustering algorithm, was used to derive the clusters of the NDVI temporal profiles for 23 time-series images in 2009. Therefore, we assumed that land cover changes from one cluster class to another were insignificant. The ISODATA algorithm initially determines a test set of cluster centers and assigns pixels to the clusters with minimum Euclidean distance in data space. In each subsequent iteration, the process first calculates the statistics of the current cluster set, then splits, merges, and deletes the clusters on the basis of modeling thresholds. After the cluster adjustment is completed, new cluster centers are determined and the process repeated. The process continues iteratively until the number of pixels with changes in each cluster falls below a change threshold or until the iteration limit is reached (Smith, 2011).

Because the optimal number of clusters in ISODATA clustering cannot be defined in advance, an estimation of the optimal number of clusters from the observed data is necessary. Using the stacked NDVI time-series image, we made a series of clustering runs by changing the number of clusters from 12 to 100. The Jefferies–Matusita (J–M) distance between defined clusters in each run was used as the measure of separability when comparing the various runs in this study (Richards, 1993). The J–M distance is asymptotic to $\sqrt{2}$, and the values $\sqrt{2}$ suggests complete separability. The average and minimum J–M distance in each run were calculated. The average J–M distance indicates the overall separability among all clusters, while the minimum J–M distance reflects the distance between most similar clusters. Therefore the optimal number of clusters used in further analysis was decided on the basis of a high average

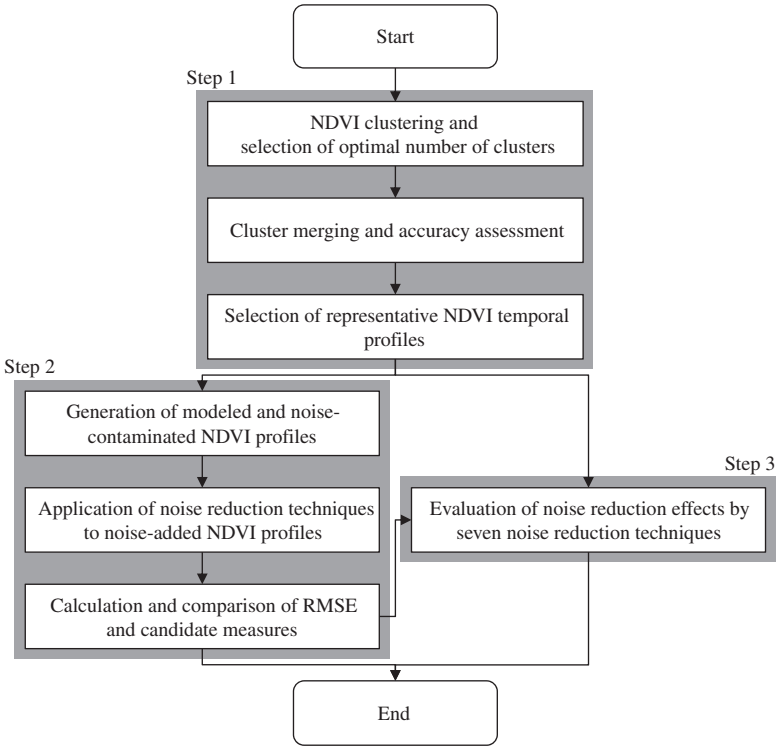

Fig. 2. Research flow.

and a high minimum J–M distance. Clustering runs were made under the following conditions for the modeling parameters determined from our expert knowledge: maximum number of iterations (10); change threshold (5%); minimum number of pixels in a class (1); maximum class standard deviation (1); minimum class distance (5); and maximum number of merge pairs (2). Sensitivity analysis of the modeling parameters was not conducted because it was not the main focus of our study.

We defined 12 thematic labels of land cover for the clusters with the references from the two high accuracy land cover classification maps derived from the TM image in 2000, the ETM+ image in 2009, and the land use map in the Jiangxi Map Collection (Editing Committee of Jiangxi Map Collection, 2008). The labels included: (1) lake/river (L/R); (2) marshland (MSL); (3) urban/sand (UR/S); (4) vegetated wetland (VW); (5) suburban/rock (SU/R); (6) cotton (COT); (7) rice paddy 1 (mixture of single- and double-cropping; RP1); (8) rice paddy 2 (single-cropping; RP2); (9) rice paddy 3 (double-cropping; PR2); (10) oil seed rape (OSR); (11) coarse needle leaf forest (CNF); and (12) dense needle leaf forest (DNF). An optimal number of clusters were merged into 12 clusters based on the J–M distance of each cluster pair and our visual inspection, and the labels were put on the clusters. The average and minimum J–M distances were again calculated for the merged 12 clusters to evaluate the separability of the clusters.

Labeling accuracy of the 12 land cover clusters was assessed through the comparison of the cluster maps with the validation samples. Because the accuracy of the samples was very important in the accuracy assessment, the samples collected accounted for the land and water cover changes. For this purpose, a number of supplemental materials described in Section 2.2, such as the field records, the time-series TM and ETM+ images, the multi-temporal high spatial resolution images, and the interview results, were used for the collection. Altogether 500 samples (refer to the second row of Table 2 for the number of samples for each clusters), collected using the stratified random sampling scheme, were used to generate a sample error matrix. Because the numbers of samples vary for different land cover clusters in the stratified random scheme, the sample error matrix was converted into a population matrix to compute unbiased statistics (Pontius and Millones, 2011). The accuracy assessment was based on the overall accuracy, kappa coefficient, producer's accuracy, and user's accuracy calculated from the population matrix.

The 10 most representative NDVI temporal profiles were selected for each land cover cluster based on the average of the root mean square error (RMSE) produced by an NDVI temporal profile when it was compared with all other temporal profiles in the cluster. Because the representative NDVI temporal profiles tended to produce low average RMSE values, the profiles with the 10 lowest values were selected as representative temporal profiles for each land cover cluster. Because we derived the clusters of the NDVI temporal profiles for 23 time-series images in 2009, we did not manage to show the clusters that changed between 2009 and other years in the clustering process. However, such profiles can be extracted as representative profiles if there is a significant number and they are distinct from other profiles. Because this measure is theoretically the same as the endmember average RMSE for the multiple endmember spectral mixture analysis (MESMA) (Dennison and Roberts, 2003), this study used VIPER Tools, a MESMA plug-in for ENVI (Roberts et al., 2007) for calculating the measures.

3.2. Development of a measure of noise reduction effects

This study developed a measure for noise reduction effects when the 'true' profiles were unavailable, by generating modeled and noise-added NDVI profiles, applying noise reduction techniques to the noise-added NDVI profiles, and calculating and comparing the RMSE and candidate measures.

The 'true' NDVI profiles were modeled by synthesizing the raw NDVI values in the representative temporal profiles selected following the procedure in Section 3.1. Taking the pixel domination of each land cover cluster summarized in the second column of Table 2 into account, we modeled the NDVI profiles for four

representative land cover types in the study area: (1) lake and river (L/R); (2) vegetated wetland (VW); (3) rice paddy 1 (RP1); and (4) coarse needle leaf forest (CNL). The modeled profile for each land cover type was generated by averaging the raw values on the same composite target dates in all the representative annual profiles of the land cover type for 11 years. Multi-year averaging could minimize the irregular spikes and drops in the original profiles. We used multi-year average profiles under the hypothesis that the class did not change in different years in the original profiles. The modeled NDVI profiles are drawn with solid black lines in Fig. 4.

Noise was artificially added to the modeled NDVI temporal profiles. In actual NDVI temporal profiles, amplitude and frequency of positive and negative noise are different, because cloud contamination, atmospheric variability, bidirectional effects, sensor viewing angles, solar angles, snow cover, and problems with instruments cause the negatively biased noise in NDVI temporal profiles (Ma and Veroustraete, 2006; Julien and Sobrino, 2010). Therefore, based on the visual interpretation of the raw NDVI temporal profiles, we experimentally generated noises with different distributions for positive and negative noise. Positive Gaussian noise with a standard deviation of 0.1 was added to each modeled temporal profile at two points (8.6% in a profile) randomly selected from the profile, and negative Gaussian noise with a standard deviation of 0.2 was added to each modeled temporal profile at seven points (30.4% in a profile) randomly selected from the profile. The noise-added NDVI profiles are drawn with the black points and dotted lines in Fig. 4.

The following seven noise reduction techniques were applied to the four noise-added NDVI temporal profiles: (1) RMMEH filter (Jin and Xu, 2013); (2) SG filter (Chen et al., 2004); (3) AG filter (Jönsson and Eklundh, 2002); (4) DL filter (Beck et al., 2006); (5) 4253HT filter (Velleman, 1980); (6) MVI filter (Ma and Veroustraete, 2006); and (7) ARM3-5 filter (Filipova-Racheva and Hall-Beyer, 2000). The characteristics of the selected noise reduction techniques are described in Table 1. Fourier-based techniques were not included because of their inability to reduce the noise of irregular or asymmetrical temporal patterns commonly seen in non-vegetation profiles (Hird and McDermid, 2009). We also excluded threshold-based techniques because of the difficulty in their threshold tuning (Lu et al., 2007). Therefore, this study compared four asymmetric function fitting techniques (SG, AG, DL, and ARM3-5 filters) and three iterative simple mathematical operation techniques (RMMEH, 4253HT, and MVI filters).

In the application of the SG filter, two modeling parameters, the half size of the smoothing window and the degree of the smoothing polynomial, were set to 4 and 2 in fitting the long-term change trend, and 3 and 3 in the iterative fitting of the NDVI profiles, respectively. AG and DL filters were applied with TIMESAT software (version 3.0; Eklundh and Jönsson, 2010). We applied an MVI filter with the setting of a 10% multi-year average as set in Hird and McDermid (2009). Three similar noise-added annual profiles were joined together, to meet the model requirements of the AG and DL filters in TIMESAT. The reconstructed profiles in the second year were extracted for further analysis.

This study regarded the RMSE as the absolute measure in the evaluation of noise reduction effects for the seven techniques. The RMSEs between the reconstructed profiles for the seven techniques and modeled profiles were derived for the four profiles of representative land cover types. The RMSEs of the representative profiles for the seven techniques were compared on the basis of land cover types and noise reduction techniques. The RMSEs were also compared with the following four measures in this analysis. All four measures range from zero to two.

The first and second measures, the distance from the resulting NDVI temporal profiles to the noise-added profiles and from the upper envelope profiles to the noise-added profiles, were developed on the basis of the two criteria introduced in Julien and Sobrino (2010). The first measure was designed to evaluate the fidelity of the reconstructed profiles to the noise-added profiles. The mean value of the average distance between the reconstructed NDVI temporal profiles and the noise-added profiles for a noise reduction technique (nr) in a cluster (c) denoted by $D_o(nr,c)$ was defined as follows:

$$D_o(nr,c) = \frac{\sum_p \sum_t |NDVI_{nr,c,t,p} - NDVI_{c,t,p}|}{n_p \cdot n_t} \quad (1)$$

where $NDVI_{nr,\,c,\,t,\,p}$ is the NDVI value reconstructed with an nr filter in cluster c at time t at location p, $NDVI_{c,\,t,\,p}$ is the original NDVI value in cluster c at time t at location p, n_p is the total number of sample locations in a cluster (set to 1 in this calculation), and n_t (set to 23 in this calculation) is the total number of time points. A smaller $D_o(nr,c)$ means a better fit to the noise-added NDVI temporal profile. The second measure was designed taking into account the decrease in the NDVI values caused by negative noise. Therefore, the measure for this criterion ($D_e(nr,c)$) was defined as the mean value of the average distance between the NDVI profiles composed of the highest NDVI values among all the NDVI values reconstructed using the seven techniques and the noise-added profiles for a noise reduction technique (nr) in a cluster (c):

$$D_e(nr,c) = \frac{\sum_p \sum_t |NDVI_{nr,c,t,p} - NDVI_{max,c,t,p}|}{n_p \cdot n_t} \quad (2)$$

where $NDVI_{max,\,c,\,t,\,p}$ is maximum NDVI value among the reconstructed values with the seven techniques in cluster c at time t at location p. A better fit to the upper envelope temporal profile can achieve a smaller $D_e(nr,c)$.

We designed the third and fourth measures to comprehensively evaluate the noise reduction effects using the above two measures by averaging them arithmetically and geometrically. The

Table 1
Noise reduction techniques selected for the comparisons.

Technique	Description
RMMEH filter (RMMEH) (Jin and Xu, 2013)	A series of running medians, arithmetic average calculation, maximum operation, endpoint processing, and weighted moving average
Iterative Savitzky-Golay filter (SG) (Chen et al., 2004)	Iterative weighted moving average filter using the weights determined with polynomial regression
Asymmetrical Gaussian function fitting (AG) (Jönsson and Eklundh, 2002)	Regression of the local fittings by nonlinear functions at intervals around local maxima and minima using a global function
Double logistic function-fitting (DL) (Beck et al., 2006)	Fitting with a double logistic function using statistical metrics
4253H, twice filter (4253HT) (Velleman, 1980)	A series of running medians with different sizes and a weighted average filter
Mean-value iteration filter (MVI) (Ma and Veroustraete, 2006)	Iterative replacements of each NDVI value with the average of NDVI values on prior and posterior dates based on a threshold value
ARMD3-ARMA5 filter (ARM3-5) (Filipova-Racheva and Hall-Beyer, 2000)	A series of an autoregressive running median filter with a window size of three and an autoregressive running mean filter with a window size of five

Table 2
Population confusion matrix of 12 merged NDVI clusters. PA and UA refer to producer's accuracy and user's accuracy. Overall accuracy and kappa coefficients were 88.7% and 0.872, respectively.

	Comparison (number of samples)													
	L/R (60)	MSL (20)	UR/S (10)	VW (40)	SU/R (20)	COT (20)	RP1 (80)	RP2 (60)	RP3 (40)	OSR (10)	CNF (80)	DNF (60)	Comp total	UA (%)
Reference (pixel population)														
L/R (35878)	0.110	0.002	0.000	0.002	0.000	0.000	0.000	0.000	0.000	0.000	0.000	0.000	0.114	96.4
MSL (13133)	0.004	0.036	0.000	0.002	0.000	0.000	0.000	0.000	0.000	0.000	0.000	0.000	0.042	85.7
UR/S (6931)	0.003	0.001	0.013	0.001	0.001	0.000	0.000	0.001	0.000	0.000	0.000	0.000	0.022	60.0
VW (24818)	0.002	0.000	0.000	0.077	0.000	0.000	0.000	0.000	0.000	0.000	0.000	0.000	0.079	97.4
SU/R (9489)	0.001	0.000	0.001	0.000	0.023	0.000	0.001	0.003	0.000	0.000	0.001	0.000	0.030	75.0
COT (11660)	0.000	0.000	0.000	0.000	0.000	0.026	0.005	0.003	0.000	0.000	0.003	0.000	0.037	70.8
RP1 (50186)	0.000	0.000	0.000	0.000	0.000	0.002	0.142	0.004	0.002	0.000	0.007	0.002	0.159	89.0
RP2 (39620)	0.000	0.000	0.000	0.000	0.002	0.002	0.007	0.106	0.002	0.000	0.007	0.000	0.126	84.5
RP3 (25451)	0.000	0.000	0.000	0.000	0.000	0.000	0.004	0.004	0.073	0.000	0.000	0.000	0.081	90.5
OSR (8070)	0.000	0.000	0.000	0.000	0.000	0.000	0.004	0.000	0.000	0.020	0.002	0.000	0.026	76.9
CNF (50788)	0.000	0.000	0.000	0.000	0.000	0.002	0.006	0.004	0.000	0.000	0.144	0.004	0.161	89.5
DNF (38976)	0.000	0.000	0.000	0.000	0.000	0.000	0.002	0.000	0.000	0.000	0.004	0.118	0.124	95.0
Ref Total	0.120	0.039	0.014	0.082	0.026	0.033	0.170	0.126	0.077	0.020	0.168	0.124	1.000	
PA (%)	91.5	91.1	91.3	93.3	86.1	80.2	83.2	84.5	94.4	100.0	86.0	94.8		

Overall accuracy (%) = 88.7.
Kappa coefficient = 0.872.
Allocation disagreement = 0.09.
Quantity disagreement = 0.03.

arithmetic mean ($D_a(nr,c)$) and geometric mean ($D_g(nr,c)$) of $D_o(-nr,c)$ and $D_o(nr,c)$ were respectively given by:

$$D_a(nr,c) = \frac{D_o(nr,c) + D_e(nr,c)}{2} \quad (3)$$

$$D_g(nr,c) = \sqrt{D_o(nr,c) + D_e(nr,c)}. \quad (4)$$

A better fit to both the upper envelope and noise-added profiles gives smaller $D_a(nr,c)$ and $D_g(nr,c)$.

The relationship between these four measures of the base RMSE was examined through calculating the correlation coefficient (R^2). R^2 was calculated for each profile using the four measures and RMSEs for all of the seven noise reduction techniques. The measure with the highest average R^2 of the four temporal profiles against the RMSEs was selected as the most appropriate measure in the evaluation of noise reduction when the 'true' profiles were not available, and was used in the analysis described in Section 3.3.

3.3. Evaluation of noise reduction effects of seven noise reduction techniques

In the last part of the analysis, this study evaluated the noise reduction effects of the seven noise reduction techniques. The seven noise reduction techniques used in the analysis described in Section 3.2 were applied to the 120 representative NDVI temporal profiles (10 profiles, 12 land cover clusters) extracted according to the procedure in Section 3.1. The quality assurance images imported from the MODIS products were used in the application of the SG filter. The same modeling parameters for the SG and MVI filters were set for this analysis. The first five NDVI values in 2000 and last five values in 2012 were excluded from the resultant NDVI temporal profiles to avoid the effects of endpoint processing for the seven techniques. Thus, the consecutive comparisons were made using the profiles for the 11 years between 2001 and 2011.

The effects of noise reduction using the seven techniques were compared against each other using the raw and reconstructed NDVI temporal profiles both visually and quantitatively. In the visual comparison, we used the most representative profiles at points 1–12 in Fig. 1. Not only were the differences in the noise reduction effects for the seven techniques examined, but also the difference for the particular techniques in the 12 land cover clusters.

The quantitative evaluation of the noise reduction effects for the NDVI temporal profiles by the seven noise reduction techniques was performed using the most appropriate measure selected according to the procedure in Section 3.2. In the calculation of the measure, n_p and n_t were set to 10 and 253, respectively. The overall performance of the noise reduction for each technique was evaluated on the basis of the average of the selected appropriate measure over the 12 land cover clusters.

4. Results

4.1. Exploration of an approach to extracting representative NDVI temporal profiles

4.1.1. NDVI clustering and selection of optimal number of clusters

Fig. 3 presents the cluster separability based on the J–M distance in the 89 separate clustering runs (12–100 clusters). The very high average J–M distance (black points and solid line in Fig. 3) indicated almost complete separability (nearly equal to $\sqrt{2}$) in all of the 89 runs, although it increased very slightly. The minimum J–M distance (gray points and solid line in Fig. 3) fluctuated at around 1.33 and it showed a decreasing trend as the number of clusters increased (gray dotted line in Fig. 3). It reached its highest peak for the run with 36 clusters. Thus, 36 is statistically the most reasonable choice for the cluster numbers in clustering the stacked NDVI time-series image.

4.1.2. Cluster merging and labeling accuracy assessment

The 36 clusters generated above were merged into 12 clusters with the reference for the J–M distance for each cluster pair and supplemental materials explained in Section 3.1. The merged clusters achieved an average J–M distance of 1.40 and a minimum J–M distance of 1.32, indicating sufficient separability for the rest of the analysis.

Table 2 shows the population confusion matrix of 12 merged NDVI clusters. The overall accuracy and kappa coefficient were 88.7% and 0.872, respectively. The producer's accuracy for the land cover clusters ranged between 80.2% (COT) and 100.0% (OSR). The lowest producer's accuracy for COT was caused by its being

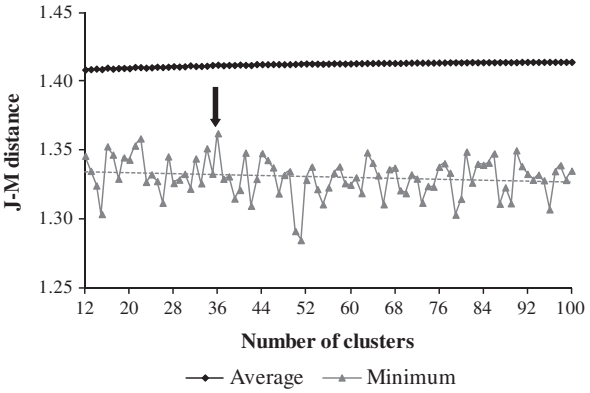

Fig. 3. Average and minimum separability based on the Jefferies–Matusita (JM) distance for the predefined numbers of NDVI clusters.

confused with RP1, RP2, and CNF. On the other hand, the user's accuracy varied more remarkably, ranging from 60.0% (UR/S) to 97.4% (VW). Misclassification of L/R, MSL, VW, SU/R, and RP2 resulted in the low user's accuracy for UR/S. The user's accuracy of 70.8% for COT stemmed from its misclassification of RP1, RP2, and CNF. Lower producer's and user's accuracy for COT suggested the difficulty in clustering the NDVI temporal profiles, merging the clusters, and labeling the clusters for this land cover type. It can be inferred that the classification accuracy in the representative clusters depended on the number of small clusters included in the merged clusters, because the representative clusters with larger variability in their profiles could cause the confusion with other clusters.

4.2. Development of a measure of noise reduction effects

4.2.1. Application of noise reduction techniques to noise-added NDVI profiles

Fig. 4 illustrates the modeled, noise-added, and reconstructed NDVI temporal profiles by the seven noise reduction techniques for the four representative land cover types. The seven noise reduction techniques showed some distinguishable characteristics in their noise reduction effects. The RMMEH and SG filters tended to show similar trends in the corrected profiles and have higher reconstructed values than the other five techniques. Consequently, they failed to minimize the positive noise at the points indicated by the arrows in Fig. 4(a) and (d). The AG and DL filters reconstructed the similar temporal profiles, but were strongly affected by both the spikes and drops of the local fluctuations that were generated by the modeled profiles and noise. These two function fitting techniques tended to underestimate the corrected values noticeably at the points around the points containing the negative noise. The other three techniques (the 4253HT, MVI, and ARM3-5 filters) excessively altered the shape and amplitude of the profiles, leading to smoother and flatter reconstructed profiles, as apparent in the profiles for the VW (Fig. 4(b)) and CNF (Fig. 4(d)). Among the three techniques, the reconstructed profiles by the 4253HT filter were closer approximations to the modeled profiles than those by the MVI and ARM3-5 filters.

4.2.2. Calculation and comparison of RMSE and candidate measures

The RMSE between the reconstructed profiles from the seven techniques and the original profiles for the four representative land cover classes are summarized in Table 3. All seven techniques achieved smaller RMSEs than the input noise-added profiles, indicating their noise reduction effects. Noise was most remarkably reduced in VW by the RMMEH and SG filters (from 0.14 to 0.06), and least noticeably reduced in L/R by the AG and DL filters (from 0.06 to 0.04). The RMMEH and SG filters generally performed best (mean value = 0.04) for the modeled profiles of defined clusters, and the AG and DL filters performed the poorest (mean value = 0.06). The 4253HT, MVI, and ARM3-5 filters showed their moderate performance in noise reduction.

The correlation coefficients (R^2) between the RMSE and the four candidate measures substituted for the RMSE are also provided in Table 3. Because of limited space, the tables for each value of the four measures were omitted. D_o was moderately correlated with the RMSE in RP1 (R^2 = 0.58), but R^2 remained low in the other cluster types. The highest R^2 was achieved by D_e in VW (0.85) and NLF (0.52), and by D_g in L/R (0.60) and RP (0.89). D_e, D_a, and D_g, obtained the moderate correlation in L/R and CNF (except for D_a in CNF), and the relatively high correlation in VW and RP1. Consequently, D_e and D_g reached a similar high mean R^2 with RMSE (0.69 and 0.70, respectively). Although the difference in the mean R^2 was very small, this study selected D_g as the most appropriate measure of noise reduction effects when the 'true' profiles were not available.

4.3. Evaluation of noise reduction effects by seven noise reduction techniques

4.3.1. Visual comparison of noise reduction effects

Fig. 5 shows the reconstructed NDVI temporal profiles using the seven noise reduction techniques in the most representative pixels for the 12 clusters. Because of limited space, only the raw and reconstructed profiles during the period between 2005 and 2007 were displayed in each figure. All seven noise reduction techniques could eliminate the anomalously high and low NDVI values in the original NDVI time-series and smooth the temporal profiles. The reconstructed profiles shared the common characteristics of the seasonal trends with those in previous studies such as Chen et al. (2004); Ma and Veroustraete (2006), and Julien and Sobrino (2010). In our visual inspection, our reconstructed profiles for RP1, RP2, RP3, CNF, and DNF had similar phenological features, such as the dates for the season start and end of growing, maximum NDVI and its timing, and average and integrated NDVI, with those in Chen et al. (2004). The reconstructed temporal profiles for UR/S, SU/R, COT, RP1, RP2, RP3, OSR, CNF, and DNF showed distinctive cyclic trends with different cycles and NDVI amplitudes. The reconstruction for UR/S clearly presented the phenological trend

Table 3
RMSE between the reconstructed profiles by the seven techniques, and the original profiles.

Cluster type	RMSE								R^2 with RMSE			
	Noise-added	RMM EH	SG	AG	DL	4253 HT	MVI	ARM 3–5	D_o	D_e	D_a	D_g
L/R	0.06	**0.02**	0.03	0.04	0.04	0.03	0.03	0.03	0.10	0.59	0.50	**0.60**
VW	0.14	**0.06**	**0.06**	0.11	0.11	0.08	0.10	0.08	0.28	**0.85**	0.75	0.83
RP1	0.08	**0.02**	0.03	0.05	0.04	0.03	0.04	0.05	0.58	0.81	0.63	**0.89**
CNF	0.09	0.04	**0.03**	0.05	0.05	0.04	0.04	0.04	0.03	**0.52**	0.19	0.48
Mean	0.09	**0.04**	**0.04**	0.06	0.06	0.05	0.05	0.05	0.25	0.69	0.52	**0.70**

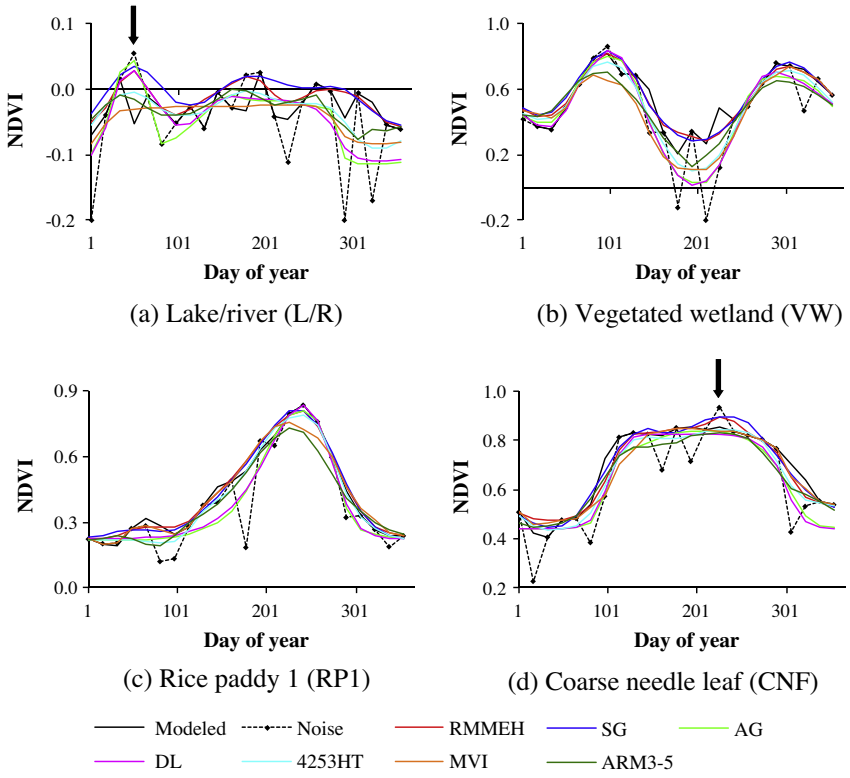

Fig. 4. Modeled, noise-added, and reconstructed NDVI temporal profiles for representative land cover types.

of urban vegetation. The cyclic trend with the two high peaks in the reconstructed profiles for COT (except for the AG and DL filter) resulted from the cultivation of cotton and its regrowth after the harvest. The reconstructed temporal profiles for L/R, MSL, and VW demonstrated the irregular trends influenced by the increase and decrease in the lake water levels. In particular, a dramatic decrease was seen in the reconstructed profile for VW because the vegetated wetland was submerged under water every year.

Although the reconstructed NDVI temporal profiles were smoother than the original profiles, the seven techniques had different effects on noise reduction. The RMMEH filter was very sensitive to the high positive outliers at the single points, such as those indicated with the black arrows in Fig. 5(c) and (g), and resulted in higher reconstructed values than the other six techniques. The reconstructed profiles using the SG filter had similar temporal trends to those using the RMMEH filter. These two techniques reconstructed the raw profiles in a different manner from the other five techniques at the small one-point spikes around the curve peaks, such as the points indicated by the white arrows in Fig. 5. The RMMEH and SG filters handled these outliers as the values approximate to the true values, while the other five filters dealt them as the values with strong positive noise. As a result, different maximum NDVI values and their timings could be derived between these two and other filters. The AG and DL filters showed their sensitivity to the high negative outliers, as seen in Fig. 5(d), (j), and (l), resulting in the production of different profiles from those using other techniques, suggesting their modeling was under-fit and over-fit. The MVI and ARM-3-5 filters generated similar temporal profiles which were flatter than the other techniques for the raw profiles with the acute high peaks and deep troughs, such as those in Fig. 5(d), (g), and (h). The corrected profiles using these filters had similar trends to those using the 4253HT filter, although the values using the former two filters were higher at the troughs and lower at the peaks than those using the latter filter.

4.3.2. Evaluation of noise reduction effects based on the new measure

Table 4 presents the evaluation results of the noise reduction effects for the seven techniques using the raw NDVI temporal profiles of twelve cluster types based on $D_g(nr,c)$. The variation of $D_g(nr,c)$ for the seven noise reduction techniques in a cluster type was smallest in UR/S (from 0.01 to 0.03) and largest in VW (from 0.06 to 0.11) and RP3 (from 0.02 to 0.07). The SG filter achieved the lowest $D_g(nr,c)$ in all twelve clusters. The RMMEH filter had the lowest $D_g(nr,c)$ in MSL, VW, SU/R, COT, RP1, CNF, and DNF and second lowest $D_g(nr,c)$ in all the other five clusters. The other five noise reduction techniques obtained higher $D_e(nr,c)$ than the SG and RMMEH filters in all 12 clusters. Specifically, the AG filter provided the highest $D_g(nr,c)$ in the seven clusters, L/R, UR/S, SU/R, COT, RP3, CNF, and DNF, and second highest $D_g(nr,c)$ in the four clusters, MSL, RP1, RP2, and OSR. $D_g(nr,c)$ for the DL filter remained up at the third highest in all twelve clusters. The 4253HT and ARM3-5 filters obtained similar $D_g(nr,c)$ in all the clusters. The 4253HT filter had the second or third highest $D_g(nr,c)$ in the eight clusters MSL, UR/S, SU/R, COT, RP1, RP2, RP3, and OSR, as did the MVI filter in the nine clusters, L/R, UR/S, SU/R, COT, RP1, RP3, OSR, CNF, and DNF. The $D_g(nr,c)$ for the ARM3-5 filter was the smallest in UR/S, VW, RP1, RP2, RP3, OSR, and DNF.

As a consequence, the RMMEH and SG filters produced the smallest average $D_g(nr,c)$ among the seven noise reduction techniques in this evaluation. Thus, this study concludes that the RMMEH and SG filters achieved the highest performance in reducing the noise in time-series NDVI profiles for the seven techniques and that they are the two most appropriate noise reduction techniques in the study area.

5. Discussion

To extract the representative and comprehensive temporal profiles, this study proposed a technical approach. The approach

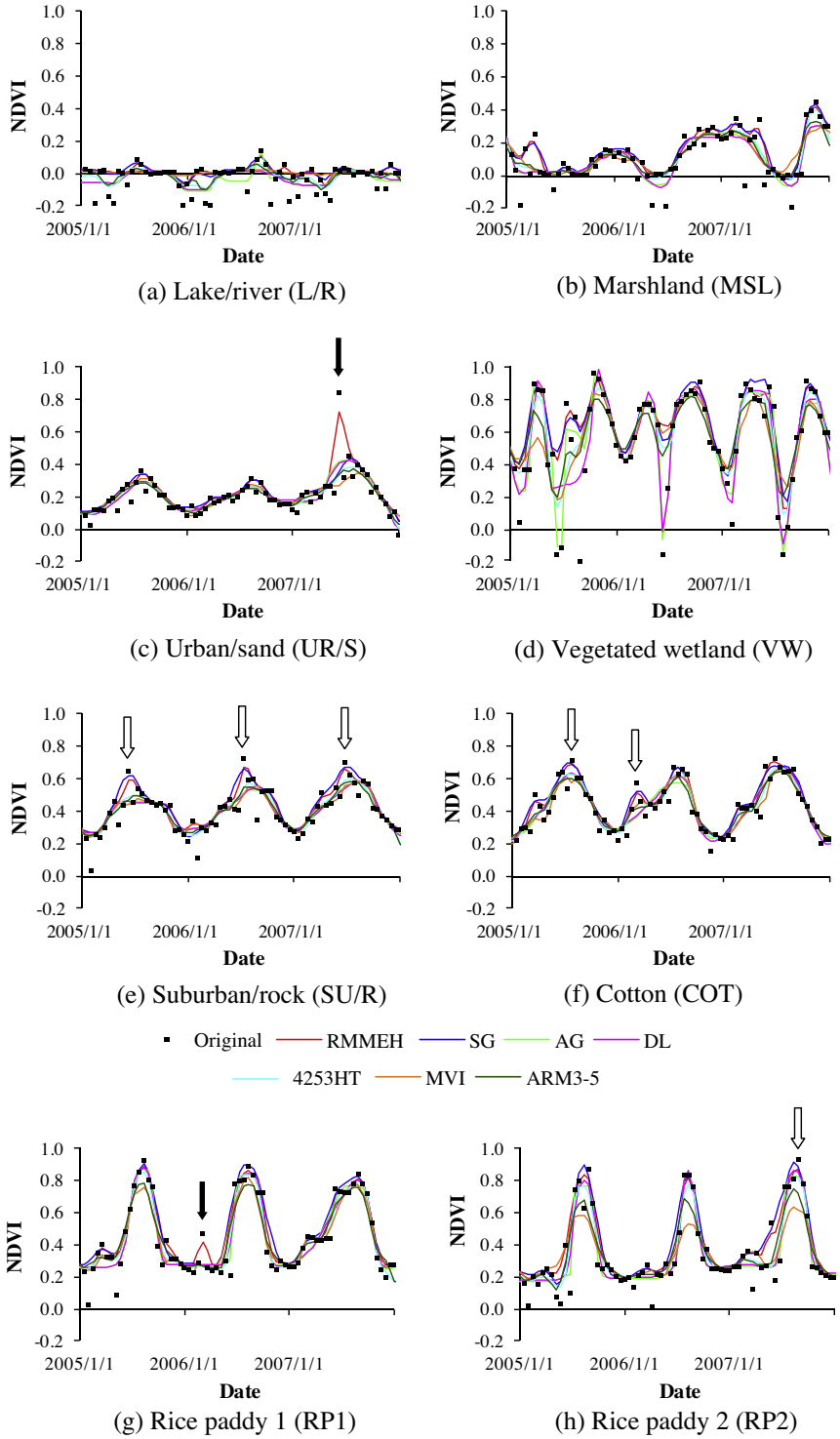

Fig. 5. (a–l) Reconstructed NDVI temporal profiles generated using the seven noise reduction methods.

consisted of NDVI profile clustering by ISODATA, cluster merging, labeling accuracy assessment, and selection of representative NDVI profiles based on the average RMSE of the cluster. Through this approach, we were able to extract 120 representative temporal profiles (12 clusters, 10 profiles per cluster). Although the selection of the optimal number of clusters based on the J–M distance in this approach was time-consuming, this unique approach could be considered to be the third approach for the selection of temporal profiles in the evaluation of noise reduction effects, in addition to the manual approach (Bradley et al., 2007) and the random sampling approach (Chen et al., 2004).

RMSE is an absolute measure in the evaluation noise reduction effects only when 'true' modeled profiles and noise-added profiles are available (Hird and McDermid, 2009). Because realistic noise-added profiles with different amplitudes and frequencies for positive and negative noise are difficult to generate, it is practical to evaluate the effects of noise reduction using observed and reconstructed profiles. However, the RMSE is a relative measure

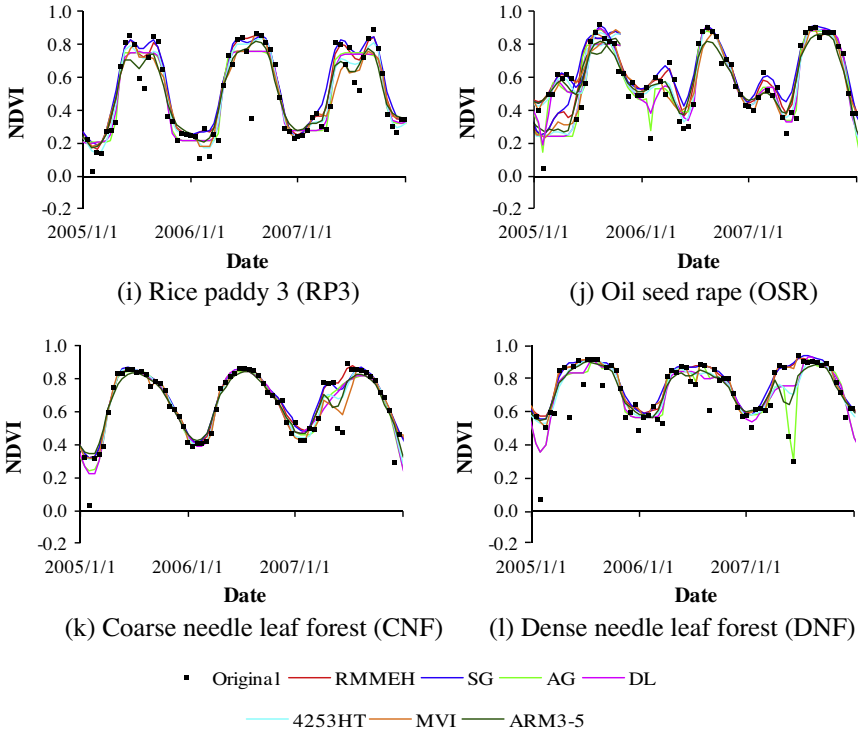

Fig. 5 (*continued*)

when observed and reconstructed profiles are used for performance evaluation of noise reduction techniques, because of the lack of 'true' profiles. Thus, we developed a new measure for noise reduction effects using observed and reconstructed NDVI profiles when 'true' profiles are unavailable. $D_g(nr,c)$ is calculated on the basis of both the distance from the resulting NDVI temporal profiles, and the distance from the upper envelope profiles, to the noise-added profiles (Julien and Sobrino, 2010). Considering the negatively-biased noise distribution in NDVI profiles, $D_g(nr,c)$ is more appropriate for the evaluation of noise reduction effects when there is no 'true' profile, than for the RMSE, which can account for the distance between the original and noise-added profiles.

Our investigation of the noise reduction effects using $D_g(nr,c)$ revealed that the RMMEH and SG filters, which achieved the highest performance for the seven techniques, were the two most appropriate techniques in the study area. The RMMEH and SG filters could reduce the negative noise more correctly than other techniques, because they were designed to preserve the upper envelopes of the profiles. However, their designs resulted in high sensitivity to the positive noise that led to the poor noise reduction effects for the positive noise, as seen by the dips in the black profile in Fig. 4(a) and (d). The AG and DL filters were not able to perform as well as in other studies (Jönsson and Eklundh, 2004; Hird and McDermid, 2009). This is particularly because the positive and negative noise added to the modeled profiles was generated with different amplitudes and frequencies. Because of this biased noise distribution in the noise-added profiles, the AG filter could not deal with the non-Gaussian noise and the DL filter failed to accurately detect the inflection points of the profiles. The

Table 4
$D_g(nr,c)$ for the evaluation of the noise reduction effects by the seven noise reduction techniques in using the temporal NDVI profiles of the twelve clusters. Bold numbers are smallest among the seven techniques.

Cluster #	Cluster type	Filter type						
		RMMEH	SG	AG	DL	4253HT	MVI	ARM3-5
1	L/R	0.03	**0.02**	0.06	0.06	0.05	0.04	0.05
2	MSL	**0.03**	**0.03**	0.06	0.07	0.05	0.06	0.06
3	UR/S	0.02	**0.01**	0.03	0.03	0.03	0.03	0.03
4	VW	**0.06**	**0.06**	0.08	0.10	0.09	0.09	0.11
5	SU/R	**0.02**	**0.02**	0.05	0.05	0.04	0.04	0.04
6	COT	**0.02**	**0.02**	0.05	0.04	0.04	0.04	0.04
7	RP 1	**0.03**	**0.03**	0.05	0.05	0.05	0.05	0.06
8	RP 2	0.04	**0.03**	0.06	0.06	0.06	0.07	0.07
9	RP 3	0.04	**0.02**	0.07	0.07	0.06	0.06	0.07
10	OSR	0.03	**0.02**	0.05	0.05	0.05	0.05	0.06
11	CNF	**0.02**	**0.02**	0.05	0.05	0.04	0.03	0.04
12	DNF	**0.02**	**0.02**	0.05	0.05	0.04	0.03	0.05
Mean		**0.03**	**0.03**	0.06	0.06	0.05	0.05	0.06

4253HT, MVI and ARM3-5 filters, that could not preserve the upper envelopes and maintain the original trends of the profiles in the running medians, also resulted in the poor noise reduction performance.

6. Conclusions

Noise reduction for the NDVI time-series is an essential process in the ecological applications such as phonology in croplands, urban, wetland, and nature lands, because these applications can be linked to the ongoing global issues including climate change, food security and health problems. This study performed empirical comparisons of the seven noise reduction techniques for the NDVI time-series based on a new measure for the situation when 'true' profiles were not available. The proposed approach to accurately extract representative NDVI temporal profiles, for all land cover types of clustered profiles, selected optimal number of clusters, merged and labeled them, and selected the representative NDVI profiles with high separability and labeling accuracy. We developed the geometric average of the mean average distance between the reconstructed profile and the raw profiles, and the mean average distance between the reconstructed profile and the upper envelope ($Dg(nr,c)$) as an appropriate measure for the evaluation of noise reduction effects using observed and reconstructed profiles. Our comparison of the seven noise reduction techniques for NDVI temporal profiles based on $Dg(nr,c)$ revealed that the RMMEH and iterative Savitzky–Golay filters were the two most appropriate noise reduction techniques for the NDVI temporal profiles of the study area.

We strongly believe that the evaluation of noise reduction effects is necessary when selecting the appropriate noise reduction techniques before conducting each application study. This is because the effects of noise reduction vary for different land cover types and study areas, as suggested by the fact that the previous comparison studies showed inconsistent results (Dijk et al., 1987; Jönsson and Eklundh, 2004; Hird and McDermid, 2009). The framework for the evaluation of noise reduction effects using the proposed approach for the accurate extraction of representative NDVI temporal profiles and ($Dg(nr,c)$) in this study is robust and applicable in the evaluation of noise reduction effects with different techniques and in other study areas. Thus, this study could serve as a guide for researchers who needed to reconstruct the NDVI temporal profiles. The framework will be applicable to the assessment of noise reduction effects in the future using newly developed techniques in future.

Future tasks to improve the framework in this study include the development of faster processing to select the optimal number of clusters in ISODATA clustering and to label the cluster names. The development of a technique to generate more realistic noise that can be added to the modeled noise is also a future area of research.

Acknowledgements

This study was supported by the Ministry of Science and Technology, China, National Research Program (2010CB530300, 2012CB955501, 2012AA12A407, 2013AA122003), and the National Natural Science Foundation of China (41271099). The authors wish to thank the editor and the anonymous reviewers for their insightful comments and constructive suggestions.

Appendix A. Supplementary material

Supplementary data associated with this article can be found, in the online version, at http://dx.doi.org/10.1016/j.isprsjprs.2014.01.003.

References

Atkinson, P.M., Jeganathan, C., Dash, J., Atzberger, C., 2012. Inter-comparison of four models for smoothing satellite sensor time-series data to estimate vegetation phenology. Remote Sens. Environ. 123, 400–417.

Beck, P.S.A., Atzberger, C., Høgda, K.A., Johansen, B., Skidmore, A.K., 2006. Improved monitoring of vegetation dynamics at very high latitudes: a new method using MODIS NDVI. Remote Sens. Environ. 100 (3), 321–334.

Bradley, B.A., Jacob, R.W., Hermance, J.F., Mustard, J.F., 2007. A curve fitting procedure to derive inter-annual phenologies from time series of noisy satellite NDVI data. Remote Sens. Environ. 106 (2), 137–145.

Chan, K., Xu, B., 2013. Perspective on remote sensing change detection of Poyang Lake Wetland. Ann. GIS 19 (4), 231–243.

Chen, J., Jönsson, P., Tamura, M., Gu, Z., Matsushita, B., Eklundh, L., 2004. A simple method for reconstructing a high-quality NDVI time-series data set based on the Savitzky-Golay filter. Remote Sens. Environ. 91 (3–4), 332–344.

Cleveland, R.B., Cleveland, W.S., McRae, J.E., Terpenning, I., 1990. STL: a seasonal-trend decomposition procedure based on loess. J. Official Stat. 6, 3–73.

Dennison, P.E., Roberts, D.A., 2003. Endmember selection for multiple endmember spectral mixture analysis using endmember average RMSE. Remote Sens. Environ. 87 (2–3), 123–135.

Dijik, A., Callis, S.L., Sakamoto, C.M., Decker, W.L., 1987. Smoothing vegetation index profiles: An alternative method for reducing radiometric disturbance in NOAA/AVHRR data. Photogramm. Eng. Remote Sens. 53, 1059–1067.

Editing Committee of Jiangxi Map Collection, 2008. Jiangxi Map Collection (Jiangxi Sheng Dituji). China Map Publications: 349P (in Chinese).

Eklundh, L., Jönsson, P., 2010. Version 3.0 Software manual: TIMESAT 3.0 – Software Manual. Lund University, 74P, <http://www.nateko.lu.se/TIMESAT/docs/timesat30_software_manual.pdf> (Last accessed 09.08.12).

Fang, J., Wang, Z., Zhao, S., Li, Y., Tang, Z., Yu, D., Ni, L., Liu, H., Xie, P., Da, L., Li, Z., Zheng, C., 2006. Biodiversity changes in the lakes of the Central Yangtze. Front. Ecol. Environ. 4, 369–377.

Filipova-Racheva, D., Hall-Beyer, M., 2000. Smoothing of NDVI time series curves for monitoring of vegetation changes in time. Ecological Monitoring and Assessment Network National Science Meeting 2000, Toronto, Ontario, Canada, January 17–22, 2000. <http://www.eman-rese.ca/eman/reports/meetings/national2000/toc_posters.htm> (Last accessed 27.02.11).

Gong, P., Wang, J., Yu, L., Zhao, Y., Zhao, Y., Liang, L., Niu, Z., Huang, X., Fu, H., Liu, S., Li, C., Li, X., Fu, W., Liu, C., Xu, Y., Wang, X., Cheng, Q., Hu, L., Yao, W., Zhang, H., Zhu, P., Zhao, Z., Zhang, H., Zheng, Y., Ji, L., Zhang, Y., Chen, H., Yan, A., Guo, J., Yu, L., Wang, L., Liu, X., Shi, T., Zhu, M., Chen, Y., Yang, G., Tang, P., Xu, B., Ciri, C., Clinton, N., Zhu, Z., Chen, J., Chen, J., 2013. Finer resolution observation and monitoring of global land cover: first mapping results with Landsat TM and ETM+ data. Int. J. Remote Sens. 34 (7), 2607–2654.

Guo, J., Penolope, V., Cao, C., Jürg, U., Zhu, H., Daniel, A., Zhu, R., He, Z., Li, D., Hu, F., 2005. A geographic information and remote sensing based model for prediction of habitats in the Poyang Lake area, China. Acta Trop. 96 (2–3), 213–222.

Hird, J.N., McDermid, G.J., 2009. Noise reduction of NDVI time series: an empirical comparison of selected techniques. Remote Sens. Environ. 113 (1), 248–258.

Huete, A., Didan, K., Miura, T., Rodriguez, E.P., Gao, X., Ferreira, L., 2002. Overview of the radiometric and biophysical performance of the MODIS vegetation indices. Remote Sens. Environ. 83 (1–2), 195–213.

Hui, F., Xu, B., Huang, H., Yu, Q., Gong, P., 2008. Modelling spatial–temporal change of Poyang Lake using multispectral Landsat imagery. Int. J. Remote Sens. 29 (20), 5767–5784.

Jin, Z., Xu, B., 2013. A novel compound smoother – RMMEH to reconstruct MODIS NDVI time series. IEEE Geosci. Remote Sens. Lett. 10 (4), 942–946.

Jönsson, P., Eklundh, L., 2002. Seasonality extraction by function fitting to time-series of satellite sensor data. IEEE Trans. Geosci. Remote Sens. 40 (8), 1824–1832.

Jönsson, P., Eklundh, L., 2004. TIMESAT – a program for analysing time-series of satellite sensor data. Comput. Geosci. 30 (8), 833–845.

Julien, Y., Sobrino, J.A., 2010. Comparison of cloud-reconstruction methods for time series of composite NDVI data. Remote Sens. Environ. 114 (3), 618–625.

Knight, J.F., Lunetta, R.S., Ediriwickrema, J., Khorram, S., 2006. Regional scale land cover characterization using MODIS-NDVI 250 m multi-temporal imagery: a phenology-based approach. GISci. Remote Sens. 43 (1), 1–23.

Lu, H., Raupach, M.R., McVicar, T.R., 2001. Decomposition of Vegetation Cover into Woody and Herbaceous Components Using AVHRR NDVI Time Series. Technical Report 35/01, CSIRO Land and Water, PO Box 1666, Canberra, 2601, Australia, 43p.

Lu, X., Liu, R., Liu, J., Liang, S., 2007. Removal of noise by wavelet method to generate high quality temporal data of terrestrial MODIS products. Photogramm. Eng. Remote Sens. 3 (10), 1129–1139.

Ma, M., Veroustraete, F., 2006. Reconstructing pathfinder AVHRR land NDVI time-series data for the Northwest of China. Adv. Space Res. 37 (4), 835–840.

Michishita, R., Gong, P., Xu, B., 2012a. Spectral mixture analysis for bi-sensor wetland mapping using Landsat TM and Terra MODIS data. Int. J. Remote Sens. 33 (11), 3373–3401.

Michishita, R., Jiang, Z., Gong, P., Xu, B., 2012b. Bi-scale comparisons of multi-temporal land cover fractions for wetland mapping. ISPRS J. Photogramm. Remote Sens. 72, 1–15.

Michishita, R., Jiang, Z., Xu, B., 2012c. Monitoring two decades of urbanization in the Poyang Lake area, China through spectral unmixing. Remote Sens. Environ. 117, 3–18.

Moody, A., Johnson, D.M., 2001. Land-surface phenologies from AVHRR using the discrete fourier transform. Remote Sens. Environ. 75 (3), 305–323.
Myneni, R.B., Keeling, C.D., Tucker, C.J., Asrar, G., Nemani, R.R., 1997. Increased plant growth in the northern high latitudes from 1981 to 1991. Nature 386, 698–702.
Niu, Z.G., Gong, P., Cheng, X., Guo, J.H., Wang, L., Huang, H.B., Shen, S.Q., Wu, Y.Z., Wang, X.F., Wang, X.W., Ting, Q., Liang, L., Zhang, L.N., Wang, L., Yao, Q., Yang, Z.Z., Guo, Z.Q., Dai, Y.J., et al., 2009. Geographical characteristics of China's wetlands derived from remotely sensed data. Sci. China, Ser. D Earth Sci. 52 (6), 723–738.
Pontius Jr., R.G., Millones, M., 2011. Death to kappa: birth of quantity disagreement and allocation disagreement for accuracy assessment. Int. J. Remote Sens. 32 (15), 4407–4429.
Richards, J.A., 1993. Remote Sensing Digital Image Analysis: An Introduction, second ed. Springer-Verlag, Berlin, 340p.
Roberts, D.A., Halligan, K., Dennison, P.E., 2007. VIPER Tools User Manual (Version 1.5), University of California at Santa Barbara, 91p, <http://www.vipertools.org/> (Last accessed 09.08.12).
Roderick, M.L., Noble, I.R., Cridland, S.W., 1999. Estimating woody and herbaceous vegetation cover from time series satellite observations. Glob. Ecol. Biogeogr. 8 (6), 501–508.
Rodgers III, J.C., Murrah, A.W., Cooke, W.H., 2009. The impact of Hurricane Katrina on the coastal vegetation of the Weeks Bay Reserve, Alabama from NDVI data. Estuaries Coasts 32 (3), 496–507.
Sellers, P.J., Tucker, C.J., Collatz, G., Los, S.O., Justice, C.O., Dazlich, D.A., Randall, D.A., 1994. A global 10 by 10 NDVI data set for global studies. Part 2: The generation of global fields of terrestrial biophysical parameters from the NDVI. Int. J. Remote Sens. 15 (17), 3519–3545.
Smith, R.B., 2011, Tutorial – Image Classification with TNTmips. MicroImages, Inc., 36p, <http://www.microimages.com/documentation/Tutorials/classify.pdf> (Last accessed 30.07.13).
Swets, D.L., Reed, B.C., Rowland, J.D., Marko, S.E., 1999. A weighted least squares approach to temporal NDVI smoothing. In: Proceedings of the American Society of Photogrammetric Remote Sensing, Portland, OR, USA, May 17–21, 1999. American Society of Photogrammetric Remote Sensing (ASPRS), Washington, DC, USA, pp. 526–536.
Velleman, P., 1980. Definition and comparison of robust nonlinear data smoothing algorithms. J. Am. Stat. Assoc. 75 (371), 609–615.
Verbesselt, J., Hyndman, R., Newnham, G., Culveno, D., 2010. Detecting trend and seasonal changes in satellite image time series. Remote Sens. Environ. 114 (1), 106–115.
Viovy, N., Arino, O., Velward, A.S., 1992. The best index slope extraction (BISE): a method for reducing noise in NDVI time-series. Int. J. Remote Sens. 13 (8), 1585–1590.
Wang, Y., Jiang, Z., Jin, Z., Tan, H., Xu, B., 2013. Risk factors of infectious diseases for backyard poultry farms in the Poyang Lake area, China. PLoS ONE 8 (6), e67366.
Zhang, Y., Hepner, G.F., Dennison, P.E., 2012. Delineation of phenoregions in geographically diverse regions using *k*-means++ clustering: a case study in the Upper Colorado River Basin. GISci. Remote Sens. 49 (2), 163–181.